ISSN 0869-5911, Petrology, 2013, Vol. 21, No. 5, pp. 507–521. © Pleiades Publishing, Ltd., 2013.

P-T Estimates and Timing of the Sapphirine-Bearing Metamorphic Overprint in Kyanite Eclogites from Central Rhodope, Northern Greece[1]

Evangelos Moulas[a], Dimitrios Kostopoulos[b], James A.D. Connolly[a], and Jean-Pierre Burg[a]
[a] *Department of Earth Sciences, ETH Zentrum, 8092 Zurich, Switzerland*
[b] *Department of Mineralogy and Petrology, National and Kapodistrian University of Athens, Panepistimioupoli Zographou, 15784 Athens, Greece*
e-mail: evangelos.moulas@erdw.ethz.ch

Received March 20, 2013

Abstract—Sapphirine-bearing symplectites that replace kyanite in eclogites from the Greek Rhodope Massif have previously been attributed to a high-pressure granulite-facies metamorphic event that overprinted the eclogitic peak metamorphic assemblage. The eclogitic mineralogy consisted of garnet, omphacitic pyroxene, rutile and kyanite and is largely replaced by low-pressure minerals. Omphacite was initially replaced by symplectites of diopside and plagioclase that were subsequently replaced by symplectites of amphibole and plagioclase. Garnet reacted during decompression to form a corona of plagioclase, amphibole and magnetite. Rutile was partly transformed to ilmenite and kyanite decomposed to produce a high-variance mineral assemblage of symplectitic spinel, sapphirine, plagioclase and corundum. The presence of quartz and corundum in the kyanite eclogites is evidence for the absence of bulk equilibrium and obviates a conventional analysis of phase equilibria based on the bulk-rock composition. To circumvent this difficulty we systematically explored the pressure-temperature-composition (P–T–X) space of a thermodynamic model for the symplectites in order to establish the pressure-temperature (P-T) conditions at which the symplectites were formed after kyanite. This analysis combined with conventional thermometry indicates that the symplectites were formed at amphibolite-facies conditions. The resulting upper-pressure limit (~0.7 GPa) of the sapphirine-producing metamorphic overprint is roughly half the former estimate for the lower pressure limit of the symplectite forming metamorphic event. Temperature was constrained ($T \sim 720°C$) using garnet-amphibole mineral thermometry. The P-T conditions inferred here are consistent with thermobarometry from other lithologies in the Rhodope Massif, which show no evidence of granulite-facies metamorphism. Regional geological arguments and ion-probe (SHRIMP) zircon dating place the post-eclogite-facies metamorphic evolution in Eocene times.

DOI: 10.1134/S0869591113050032

INTRODUCTION

The Rhodope Massif is a metamorphic nappe pile that belongs to the Alpine-Himalayan suture and collision system (e.g. Ricou et al., 1998; Burg, 2012 and references therein). High-pressure rocks from the intermediate thrust sheets contain evidence of polymetamorphic evolution at ultrahigh-pressure (UHP), high-pressure and amphibolite-facies conditions (Liati and Mposkos, 1990; Mposkos and Liati, 1993; Liati and Seidel, 1996; Mposkos and Kostopoulos, 2001). The pressure-temperature (P-T) evolution of these rocks is of geodynamic interest because it elucidates the processes of burial and uplift in convergent tectonic settings. Quartz-bearing kyanite eclogites from the intermediate thrust sheets were investigated in order to deduce their retrograde P-T path and constrain their geodynamic evolution. This study focuses on sapphirine-spinel-corundum-plagioclase-bearing symplectites after kyanite that were formed during the post-eclogite stage of the metamorphic evolution.

The observation that the rock contains both corundum and quartz, but that these phases are always separated by plagioclase indicates that the rock mineralogy does not represent bulk equilibrium. The absence of bulk equilibrium precludes analysis of phase relations on the basis of the bulk-rock composition. As an alternative we assume that the symplectites after kyanite record mosaic equilibrium (Korzhinsky, 1959), in which case the local composition that dictated mineral chemistry is unknown and most likely varied during symplectite formation. The corundum-bearing symplectites replacing kyanite are a case in point. The presence of corundum in the symplectites suggests that they are not in equilibrium with the quartz-bearing matrix moreover, the presence of sapphirine, plagioclase and spinel suggests that the reaction site around kyanite has gained MgO, FeO, Na_2O and CaO from the surrounding matrix and therefore that the

---

[1] The article is published in the original.

effective bulk composition of the kyanite domains varied with time. To establish the P-T conditions of symplectite formation our approach here is to explore the range of conditions at which the addition of the aforementioned components would reproduce the observed symplectitic mineral assemblage after kyanite.

We begin by describing briefly the petrography and mineral chemistry of the high-pressure rocks (eclogites). Then, we discuss the petrological interpretation of the symplectites and present our thermodynamic analysis for the symplectites based on Gibbs free-energy minimization. This analysis constrains the P-T conditions during retrogression and decompression of the high-pressure metamorphic rocks to $T \sim 720°C$ and $P < 0.7$ GPa. To constrain the timing of this retrogression, we then present ion-probe (SHRIMP) zircon dating that places the post-eclogite-facies metamorphic evolution in Eocene times, coeval with the magmatic activity in the region. This dating is relevant because it constrains the regional geodynamic settings in which the metamorphic overprint could have taken place. We conclude with a discussion of possible scenarios in the light of our P-T estimates, which indicate that the sapphirine-bearing symplectites formed at high-grade amphibolite-facies conditions.

GEOLOGICAL SETTING

The Rhodope Massif is a region belonging to the Alpine-Himalayan orogen (e.g. Burg, 2012 and references therein). It involves three main units (Fig. 1) namely, and according to their present-day structural position, the Upper, Intermediate and Lower Terranes (e.g. Burg et al., 1996). This terrane subdivision summarizes the results of previous works in the Bulgarian and Greek Rhodope (e.g. Burg et al., 1990; Papanikolaou and Panagopoulos, 1981, respectively). These three units were intensely deformed in a non-coaxial deformation regime and are separated by ductile mylonitic zones with regional top-to-SSW sense of shear (Burg et al., 1990; Burg et al., 1996). The studied kyanite eclogite crops out near Thermes (Fig. 1) as isolated boudins within amphibolite-facies mylonitic orthogneisses. The orthogneisses are strongly foliated and occasionally have a migmatitic texture. Ion microprobe (SHRIMP) zircon dating from the eclogites and from the leucosomes has provided two ages, 42.2 ± 0.9 and 40.0 ± 1.0 Ma (Liati and Gebauer, 1999); these latter authors interpreted these two dates as the age of the high-pressure (1.9 GPa) metamorphism of the eclogite and the age of migmatitisation of the orthogneisses, respectively. Ductile normal faulting related to regional extension was identified by structural studies (Burg et al., 1990; Koukouvelas and Doutsos, 1990; Kolocotroni and Dixon, 1991) while Jones et al. (1992) pointed out the probable relationship between the voluminous Tertiary magmatism and the extensional collapse of the Hellenic orogen. The southern Rhodope is now viewed as a metamorphic core complex (Dinter and Royden, 1993; Sokoutis et al., 1993; Brun and Sokoutis, 2007). Syn- to post-orogenic extension began in Paleocene-early Eocene in the northeastern Rhodope Massif (Bonev et al., 2006) whereas in the central Rhodope extension started in the Mid-Eocene (Lips et al., 2000; Brun and Sokoutis 2007; Wüthrich, 2009) and structured the mid-Eocene (48–43 Ma) to Oligocene marine basins (Krohe and Mposkos, 2002). Miocene extension, related to slab-retreat and formation of the Aegean Sea has produced fault-bounded grabens, predominantly on the southern side of the Rhodope Massif.

Kyanite-bearing eclogites belonging to the intermediate thrust units (eclogite-metabasic-gneiss sequence of Burg et al., 1996) were investigated to trace their metamorphic P-T path during post-high-pressure conditions. The thin sections studied here come from a 4 m long boudin near Thermes village (RH506; N 41°21′36.24″/E 24°57′56.88″). These eclogites were reported to record a complex polymetamorphic history including high-pressure metamorphic conditions (1.9 GPa and 700°C) followed by high-pressure granulite-facies ($P > 1.5$ GPa, $T > 800°C$) and amphibolite-facies conditions ($P = 0.8$–1.1 GPa, $T = 580$–690°C, Liati and Seidel, 1996).

ANALYTICAL METHODS

Major-element mineral analyses and elemental maps were obtained at ETH-Zürich and the Institut für Geowissenschaften, Johannes Gutenberg-Universität, Mainz. At ETH-Zürich a Jeol JXA 8200 electron probe used while a Jeol JXA 8900RL was used at the Institut für Geowissenschaften, Johannes Gutenberg-Universität, Mainz. Both microprobes are equipped with 5 wavelength-dispersive spectrometers operating at an accelerating voltage of 15 kV and were operated with a 2 μm beam diameter and 20 nA beam current. Natural and synthetic materials were used as standards and a CITZAF correction procedure was applied. The whole-rock composition of the studied samples was obtained using a Pananalytical Axios wavelength dispersive XRF spectrometer (WDXRF, 2 kV) at ETH-Zürich.

Zircon separation was done at the Max-Planck Institut für Chemie, Mainz, Germany. The samples were crushed with a hydraulic press and ground in a rotary mill. Zircons were extracted using a Wilfley table, Franz isodynamic magnetic separator, heavy-liquid (methylene iodide) separation and finally hand-picking under a binocular microscope. Selected zircon grains were mounted together with zircon standard grains 91500 and TEMORA 1 in epoxy resin, they were then sectioned and polished to approximately half their original thickness, gold-coated, and investigated using cathodoluminescence (CL) imaging.

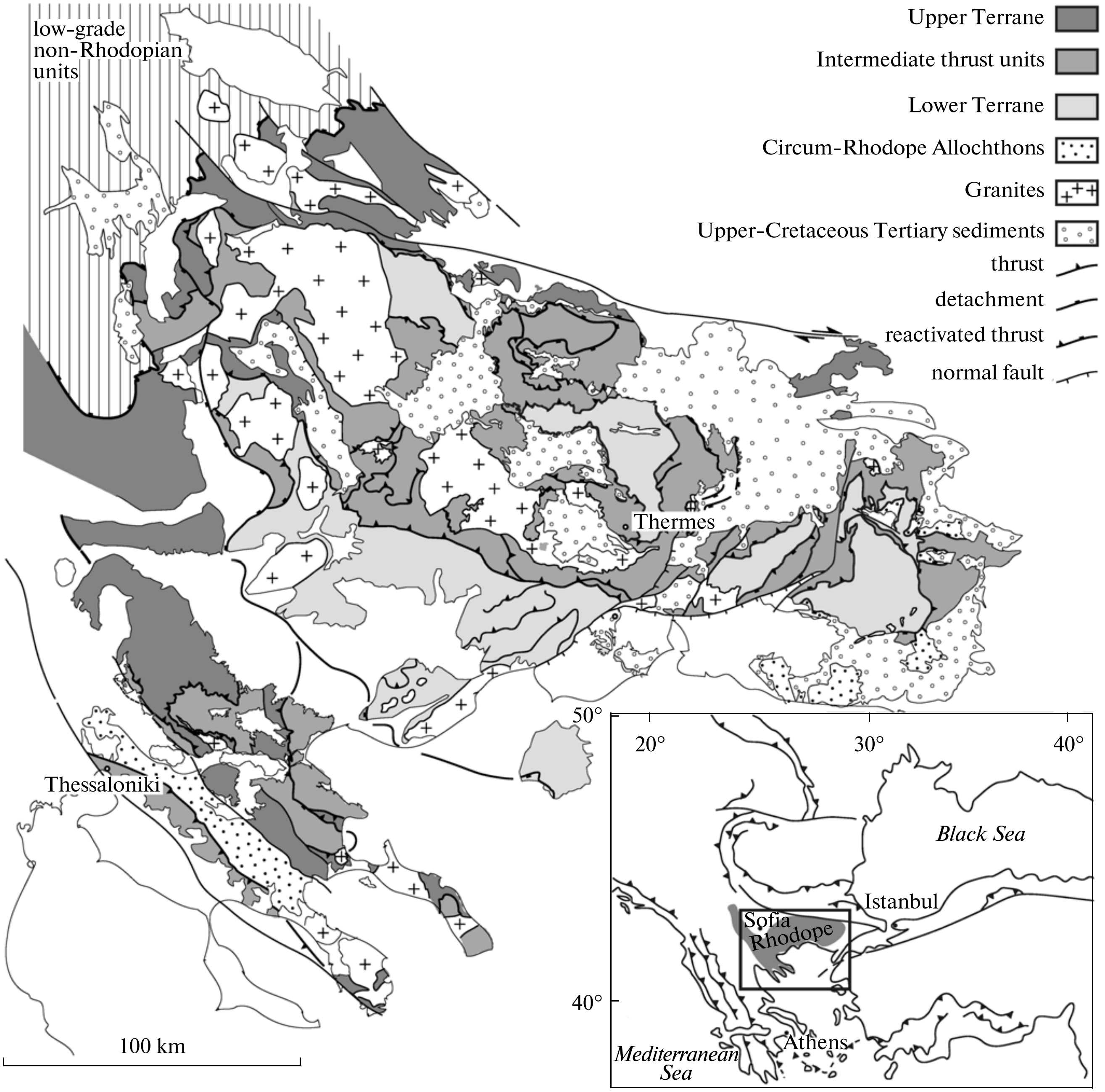

Fig. 1. Simplified geological map of the Rhodope Massif showing the main tectonic units and the sampling area near Thermes, after Burg (2012). Geographic location of the Rhodope Massif is shown on the insert.

In-situ U-Pb isotope analyses were made with the SHRIMP-II at the Center of Isotopic Research (CIR) at VSEGEI, St. Petersburg, Russian Federation, applying a secondary electron multiplier in peak-jumping mode following the procedure described by Williams (1998) and Larionov et al. (2004). A primary beam of molecular oxygen was employed to bombard zircon in order to extract secondary ions. A 70 μm Kohler aperture allowed focusing of the primary beam so that the ellipse-shaped analytical spot had a size c. 27 × 20 μm, and the corresponding ion current varied from 3.7 to 4.5 nA. The sputtered secondary ions were extracted at 10 kV. The 80 μm wide slit of the secondary ion source, in combination with a 100 μm multiplier slit, allowed mass-resolution $M/\Delta M > 5000$ (1% valley); thus, all the possible isobaric interferences were resolved. Rastering for 1 minute over a rectangular area of c. 35 × 30 μm was done before each analysis in order to remove the gold coating and possible surface common Pb contamination. The following

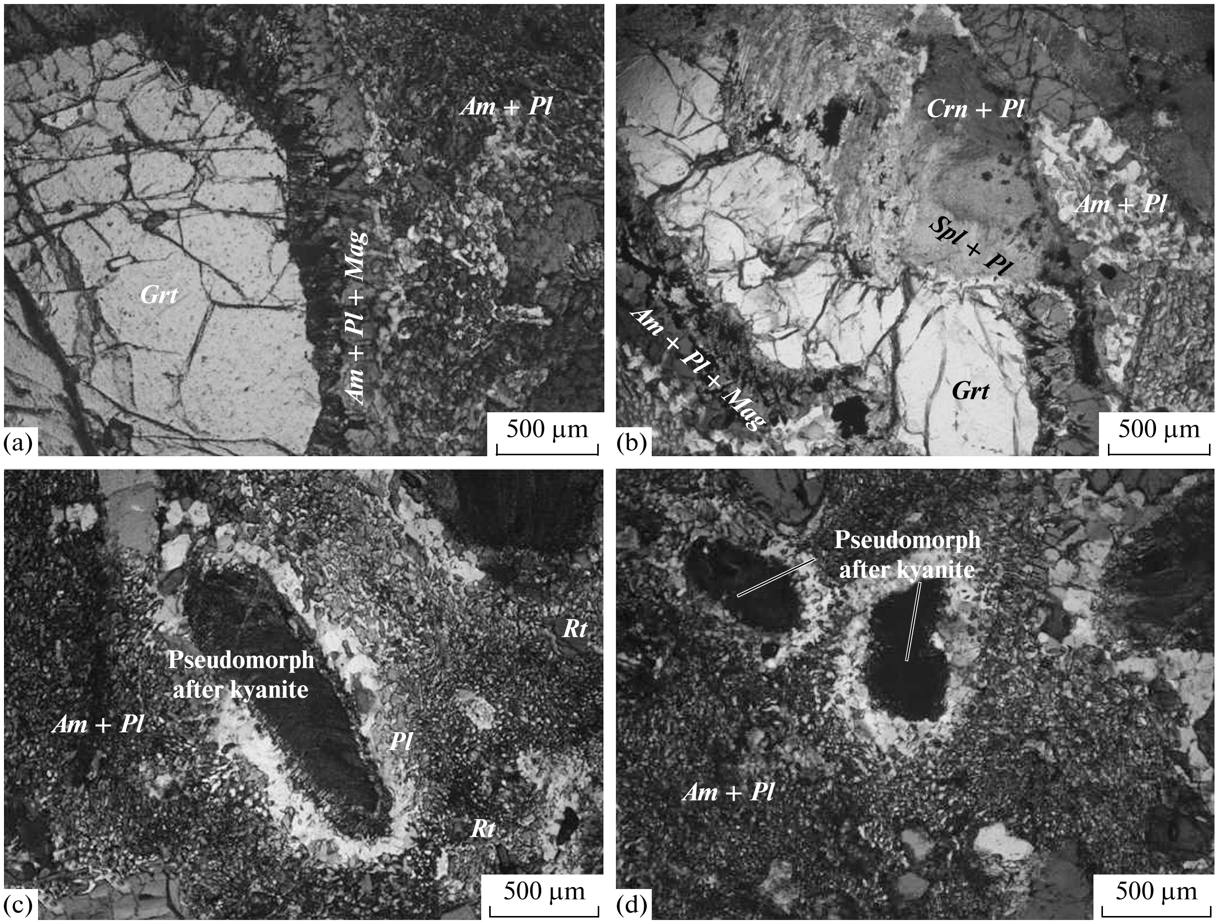

Fig. 2. Photomicrographs displaying the most important textures for our analysis (plane-polarized light—Mineral abbreviations after Siivola and Schmid (2007)). (a) Garnet porphyroblast rimmed by a corona of amphibole, plagioclase and magnetite. Note that symplectites of amphibole and plagioclase constitute most of the rock's matrix. (b) Fragment of a garnet porphyroblast and its corona replaced by spinel and plagioclase symplectites. (c) and (d) Pseudomorphs after kyanite composed of fined-grained spinel-sapphirine-corundum-plagioclase symplectites.

ion species were measured in sequence: $^{196}(Zr_2O)$—^{204}Pb-background (c. 204 AMU)—^{206}Pb—^{207}Pb—^{208}Pb—^{238}U—^{248}ThO—^{254}UO with integration time ranging from 2 to 14 seconds. Four cycles for each analyzed spot were acquired. Apart from "unknown" zircons, every fifth measurement was made on the zircon Pb/U standard TEMORA 1 (Black et al., 2003). TEMORA 1 has an accepted $^{206}Pb/^{238}U$ age of 416.75 ± 0.24 Ma. The 91500 zircon with U concentration of 81.2 ppm and a $^{206}Pb/^{238}U$ age of 1065.4 ± 0.3 Ma (Wiedenbek et al., 1995) was applied as a "U-concentration" standard.

CL-dark areas of the 'unknown' zircons were preferably chosen for the U-Pb analyses. The results collected were then processed with the SQUID vl.12 (Ludwig, 2005a) and ISOPLOT/Ex 3.22 (Ludwig, 2005b) software, with decay constants of Steiger and Jäger (1977). The common lead correction was done on the basis of measured $^{204}Pb/^{206}Pb$ and modern (i.e. 0 Ma) Pb isotope composition, according to the model of Stacey and Kramers (1975).

PETROGRAPHIC OBSERVATIONS AND MINERAL CHEMISTRY

The studied samples are mainly composed of garnet porphyroblasts in a symplectitic matrix of clinopyroxene and amphibole with plagioclase (Fig. 2a). Garnets reach up to 2 cm in diameter while amphibole-clinopyroxene-plagioclase symplectites are typically tens of μm long and 10 to 15 μm wide. Diablastic amphibole up to 500 μm in length and coarse-grained quartz are present in the matrix. Kyanite, rutile, zircon apatite and rare phengite and biotite are accessory mineral phases. Electron microprobe mineral analyses are given in Tables 1 and 2. Garnet porphyroblasts are chemically zoned (Prp_{20-39}; Grs_{14-22}; Alm_{43-54}; Sps_{1-7}) with cores rich in grossular, almandine and spessartine components while the pyrope content increases outward (Fig. 3, Table 1). The garnets are surrounded by coronae of pargasitic amphibole, plagioclase, magnetite and, occasionally, sodic gedrite. Rutile, quartz, amphibole, and plagioclase are common inclusions in garnet.

Table 1. Representative electron microprobe analyses. The whole-rock chemical composition is also given

Component	Garnet			Clinopyroxene		Plagioclase		Sapphirine	Spinel	Whole rock
	core	rim	fragment in matrix	with plagioclase		in quartz-rich domains	in corundum-rich domains	in corundum-rich domains	in corundum-rich domains	
SiO_2	39.38	39.86	39.08	52.88	54.06	66.35	58.11	11.09	0.00	53.02
TiO_2	0.06	0.04	0.10	0.08	0.09	0.01	0.01	0.01	0.02	1.17
Al_2O_3	22.22	22.18	21.72	2.06	1.79	21.56	26.62	65.79	62.24	17.17
Cr_2O_3	0.11	0.04	0.02	0.05	0.05	0.03	0.00	0.16	0.05	0.04
FeO_{total}	22.81	22.58	23.59	7.10	7.19			6.85	24.57	
$Fe_2O_{3\ total}$						0.20	0.20			7.54
MnO	1.16	1.17	0.79	0.10	0.07	0.01	0.00	0.03	0.17	0.16
MgO	7.53	8.04	6.75	13.29	13.70	0.00	0.00	16.00	13.62	7.96
CaO	7.88	7.48	8.01	22.39	22.42	2.07	8.73	0.05	0.08	7.87
Na_2O	0.02	0.05	0.04	1.14	1.44	10.04	6.51	0.01	0.00	4.03
K_2O	0.00	0.00	0.00	0.00	0.00	0.06	0.04	0.00	0.00	0.32
Total	101.16	101.43	100.10	99.08	100.80	100.34	100.22	100.00	100.75	99.28
Calculated mineral formulae to 12[O] atoms for garnet, 6 for clinopyroxene, 8 for plagioclase, 20 for sapphirine and 4 for spinel. Ferric iron-content estimated by charge balance										
Si	2.99	3.01	3.01	1.97	1.97	2.90	2.59	1.32	0.00	
Ti	0.00	0.00	0.01	0.00	0.00	0.00	0.00	0.00	0.00	
Al	1.99	1.97	1.97	0.09	0.08	1.11	1.40	9.21	1.92	
Cr	0.01	0.00	0.00	0.00	0.00	0.00	0.00	0.02	0.00	
Fe^{3+}	–	–	–	0.05	0.07	0.01	0.01	–	0.08	
Fe^{2+}	1.45	1.43	1.52	0.17	0.15	–	–	0.68	0.46	
Mn	0.07	0.07	0.05	0.00	0.00	0.00	0.00	0.00	0.00	
Mg	0.85	0.9	0.77	0.74	0.75	0.00	0.00	2.83	0.53	
Ca	0.64	0.61	0.66	0.89	0.88	0.10	0.42	0.01	0.00	
Na	0.00	0.01	0.01	0.08	0.10	0.85	0.56	0.00	0.00	
K	0.00	0.00	0.00	0.00	0.00	0.00	0.00	0.00	0.00	
Total	8.01	8.00	8.00	4.00	4.00	4.97	4.98	14.07	3.00	

Note: Analyses in wt %.

Diopsidic clinopyroxene is observed in the matrix together with amphibole and plagioclase symplectites. The clinopyroxene Na content is between 0.06 and 0.17 atoms per formula unit (apfu, Table 1). The molar ratio Mg/(Mg+Fe) (Mg#) of the clinopyroxenes ranges between 0.77 and 0.80. Diablastic amphiboles have generally a pargasitic composition with $Na(M4)_{0.06-0.20}$ decreasing towards the rim (Table 2). Symplectitic amphiboles range from pargasite through hornblende to actinolite with $Na(M4)_{0.05-0.26}$.

Corundum-plagioclase, spinel-plagioclase and sapphirine-plagioclase symplectites have overgrown kyanite crystals forming pseudomorphs (Figs. 2, 4). Kyanite and its pseudomorphs are always separated from quartz by plagioclase, which is strongly zoned (Fig. 5) with the most calcic compositions adjacent to kyanite (An_{40-84}) and the least calcic next to quartz (An_{0-40}). With regard to sapphirine, its fine-grained nature in the symplectites allowed us to obtain only two chemical analyses from different domains. Both analyses are identical and indicate an Mg# of 0.81. The modal amount of sapphirine within the kyanite pseudomorphs is less than 5% in the studied samples. The analyzed spinel crystals are generally a solid solution between spinel ($MgAl_2O_4$) and hercynite ($FeAl_2O_4$) and can be described by the formula: $(Mg_{0.53-0.54}Fe^{2+}_{0.45-0.47})Al_{1.92-1.95}Fe^{3+}_{0.05-0.08}O_4$ (ferric iron content estimated by charge balance).

GEOCHRONOLOGY

Zircons separated from the kyanite eclogite RH506 were rounded to elongated, their length measuring between 60 and 150 μm. In CL images (Fig. 6a) they display a uniform dark grey colour with no inherited cores or oscillatory zoning but occasional very thin bright rims due to Pb loss. Their Th/U ratios are extremely low (< 0.1; see Table 3), typical of metamor-

Table 2. Representative electron microprobe analyses of amphiboles from texturally different domains. Normalized according to Dale et al. (2005)

	Domain						
Component	diablastic crystal		with plagioclase symplectites			in garnet corona	
	core	rim	clinoamphibole			orthoamphibole	
SiO_2	43.63	43.13	54.20	42.53		39.12	38.9
TiO_2	0.50	0.67	0.17	0.28		0.04	0.04
Al_2O_3	15.18	13.34	2.37	18.30		21.60	21.60
Cr_2O_3	0.00	0.00	0.12	0.05		0.03	0.06
FeO_{total}	11.01	11.43	8.45	12.42		15.70	15.45
MnO	0.19	0.09	0.09	0.15		0.45	0.50
MgO	14.10	14.28	18.95	11.15		17.20	17.17
CaO	9.24	11.32	12.07	8.56		0.71	0.67
Na_2O	3.44	2.84	0.82	3.75		3.43	3.42
K_2O	0.60	0.69	0.06	0.70		0.01	0.01
Total	97.89	97.81	97.29	97.89		98.29	97.82
Si	6.24	6.26	7.66	6.12		5.57	5.56
Ti	0.05	0.07	0.02	0.03		0.00	0.00
Al	2.56	2.28	0.39	3.11		3.62	3.64
Cr	0.00	0.00	0.01	0.01		0.00	0.01
Fe^{3+}	0.58	0.35	0.20	0.41		0.51	0.50
Fe^{2+}	0.73	1.03	0.80	1.08		1.36	1.35
Mn	0.02	0.01	0.01	0.02		0.05	0.06
Mg	3.00	3.09	3.99	2.39		3.65	3.66
Ca	1.42	1.76	1.83	1.32		0.00	0.00
Na	0.95	0.80	0.22	1.05		0.00	0.00
K	0.11	0.13	0.01	0.13		0.00	0.00
Total	15.67	15.80	15.14	15.67		15.83	15.84
Na(M4)	0.20	0.06	0.05	0.26	Na(A)	0.83	0.83
Al(T)	1.76	1.74	0.34	1.88	Al(T)	2.43	2.44

Note: Analyses in wt %.

phic zircons (Teipel et al., 2004). Their $^{206}Pb/^{238}U$ ages spread between 40.9 ± 1.7 and 67 ± 5.8 Ma whereas three grains define a Terra-Wasserburg concordant age of 42 ± 2 Ma (Fig. 6b). Two other grains yield a concordant age of approximately 55–60 Ma.

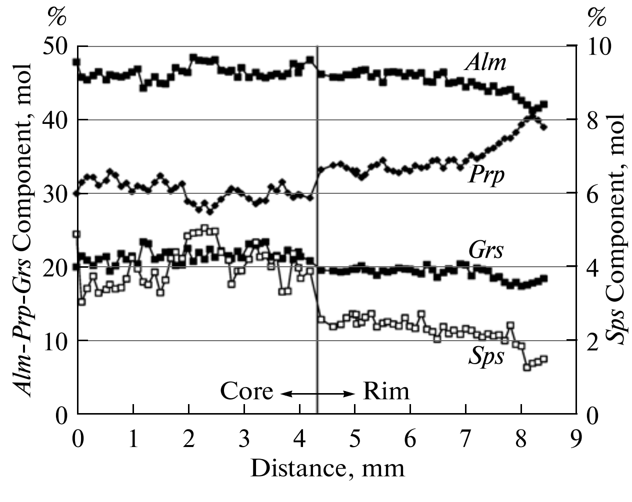

Fig. 3. Compositional profiles across garnet porphyroblast. Two compositionally different domains (core and rim) can be distinguished. The grossular, spessartine and almandine components decrease towards the rim of the garnet while the pyrope component increases.

ESTIMATION OF *P-T* CONDITIONS

Conventional Geothermometry

The application of geothermometers to constrain metamorphic conditions is restricted to mineral assemblages that are assumed to represent relict equilibrium (Powell and Holland, 2008). The garnet-clinopyroxene thermometer (e.g. Ellis and Green, 1979) and the GASP barometer (e.g. Holdaway, 2001) are commonly used to estimate temperature and pressure during metamorphism, respectively. Unfortunately, in the studied samples, garnet and clinopyroxene were never found in contact. The GASP barometer cannot be used because kyanite (the only Al_2SiO_5 phase observed) is part of locally re-equilibrated corundum-spinel-sapphirine bearing domains and thus not in equilibrium with garnet and plagioclase in the matrix.

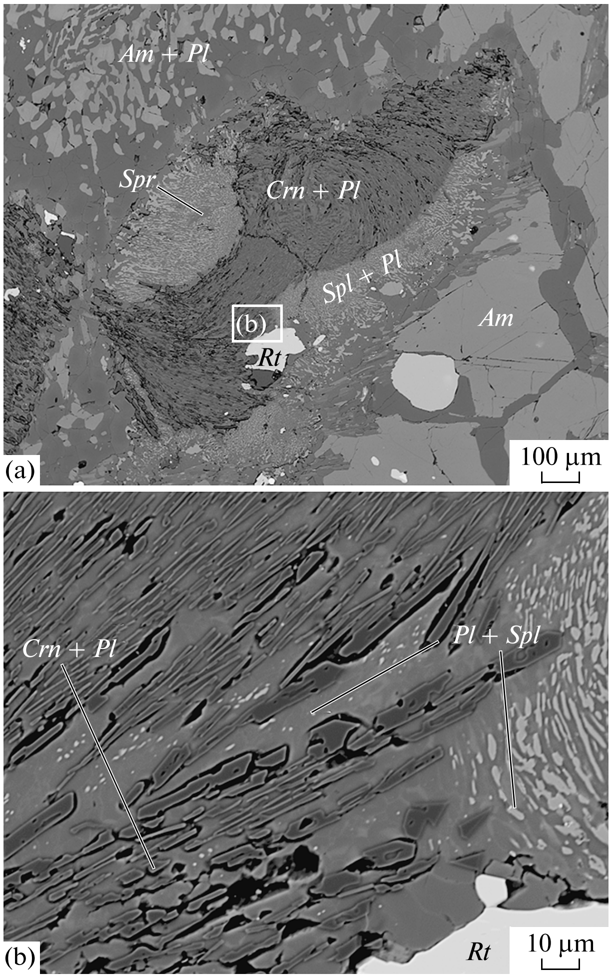

Fig. 4. (a) Backscattered electron (BSE) image of a pseudomorphs after kyanite. (b) Detail of (a) showing the fine-grained nature of the symplectites that replace kyanite.

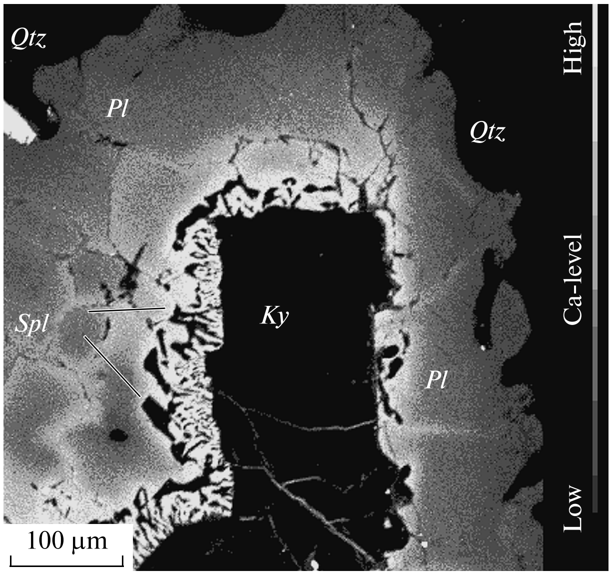

Fig. 5. Calcium map of plagioclase armouring kyanite and showing anorthite-rich compositions next to the aluminosilicate phase (kyanite) and albitic composition next to quartz. The spinel occurs in the Ca-rich domain.

However, garnet-amphibole thermometry (Graham and Powell, 1984; Perchuk, 1991) can be used to estimate the temperature of the amphibole corona formation. Twenty seven garnet-amphibole pairs from the garnet corona were identified and analyzed. The resulting temperature estimate is 713 ± 60°C and 733 ± 66°C using the thermometers of Graham and Powell (1984) and Perchuk (1991) respectively (Fig. 7). The abundance of these minerals and their presence in contact reduces the uncertainties caused by disequilibrium.

Metamorphic Evolution and Mass Transfer Constrains

Eclogites are plagioclase-free rocks composed mainly of garnet and omphacite (e.g. Carswell 1990). The presence of amphibole and plagioclase in coronae around garnet (Fig. 2a) and the symplectitic intergrowths of clinopyroxene with plagioclase indicate recrystallization in the plagioclase stability field during decompression (e.g., Godard 2001 and references therein). The high-pressure mineral assemblage is mostly constituted of garnet and sodic clinopyroxene (omphacite) with rutile and kyanite as accessory phases. The lack of evidence for partial melting and the stability of amphibole during decompression constrain the maximum temperature of the metamorphic overprint to $T < 1050$°C (Rapp et al., 1991; Rushmer, 1991). The preserved zoning in garnet also suggests that post-eclogite equilibration temperatures were insufficient for extensive diffusive re-equilibration (e.g. Anderson and Olimpio, 1977; Woodsworth, 1977; Florence and Spear, 1991; Spear and Florence, 1992; Caddick et al., 2010). Symplectites of plagioclase with corundum, sapphirine and spinel replace kyanite in the post-eclogite metamorphic overprint, the *P-T* conditions of which are the subject of the present work.

The crystallisation of spinel and plagioclase as a result of kyanite breakdown requires an influx of Na_2O, CaO, FeO and MgO at the kyanite-quartz interface (Fig. 5). Based on textural observations, there are no other Fe–Mg-bearing phases than spinel and sapphirine in the kyanite domains (Fig. 4a). Given the phase relationships in studied thin sections, garnet and its corona minerals have most likely supplied Fe and Mg for the formation of the spinel-plagioclase symplectites in the kyanite pseudomorphs (Fig. 2b) indicating that the source of these elements was local. This influx of elements is therefore a micro-scale metasomatic process. A similar process has been doc-

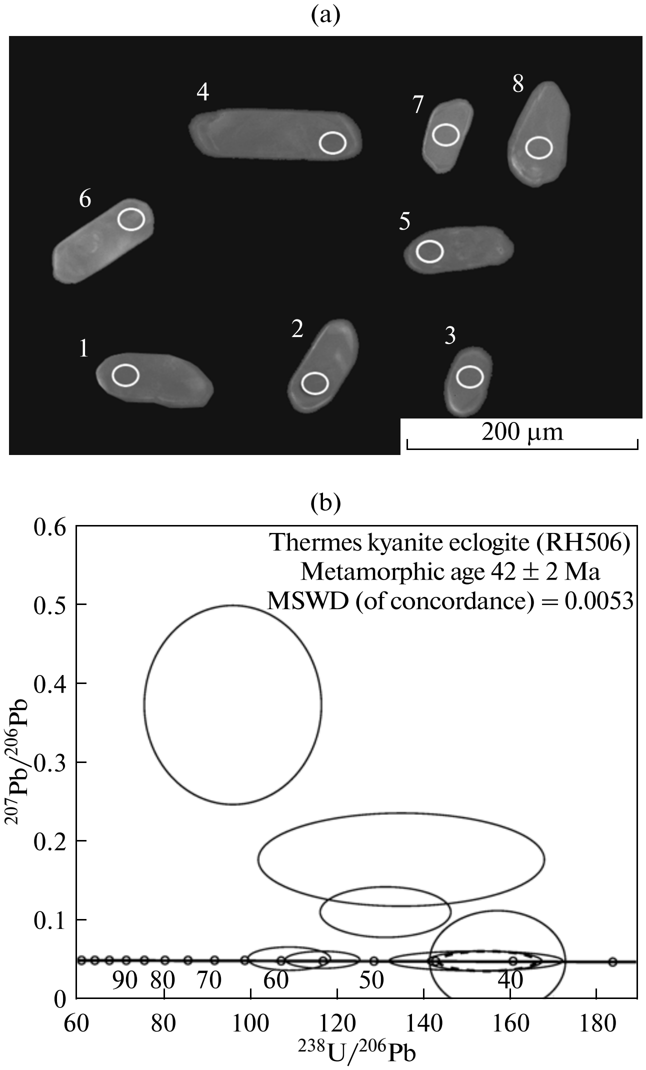

Fig. 6. (a) Cathodoluminescence (CL) image of zircon grains separated from the Thermes kyanite eclogite. (b) Tera-Wasserburg diagram for measured zircons from the Thermes kyanite eclogite and calculated concordia age of 42 ± 2 Ma, (2σ, decay-constant errors included, probability of concordance 0.94). Two zircon dates yield a concordant age of around 55–60 Ma.

umented for assemblages in felsic (e.g., Tajčmanová et al., 2007, 2011) and mafic compositions (e.g., Liati and Seidel, 1996; Godard and Mabit, 1998; Nakamura and Hirajima, 2000). These works emphasized that the absence of contacts between quartz and kyanite and the crystallization of plagioclase in between require a difference in the chemical potentials of SiO_2 and Al_2O_3 across plagioclase (Fig. 8). The presence of corundum coupled with the absence of a silica polymorph in the kyanite-breakdown domains indicates that these domains are saturated in Al_2O_3 and undersaturated with respect to SiO_2, although the presence of quartz indicates that the rest of the rock is saturated in SiO_2. Local SiO_2 undersaturation in quartz-bearing rocks has also been reported by Aranovich and Kozlovskii (2009) who pointed out the necessity of constraining silica activity before conclusions on *P*-*T* conditions are drawn. Therefore, the investigation of local mineral equilibria is necessary to deduce the *P*-*T* conditions of the breakdown of kyanite.

Thermodynamic Modeling of Kyanite Breakdown

The crystallization of corundum during kyanite breakdown and the formation of distinct textural domains in the rock where corundum and quartz are never in contact (e.g. Fig. 5) indicate the development

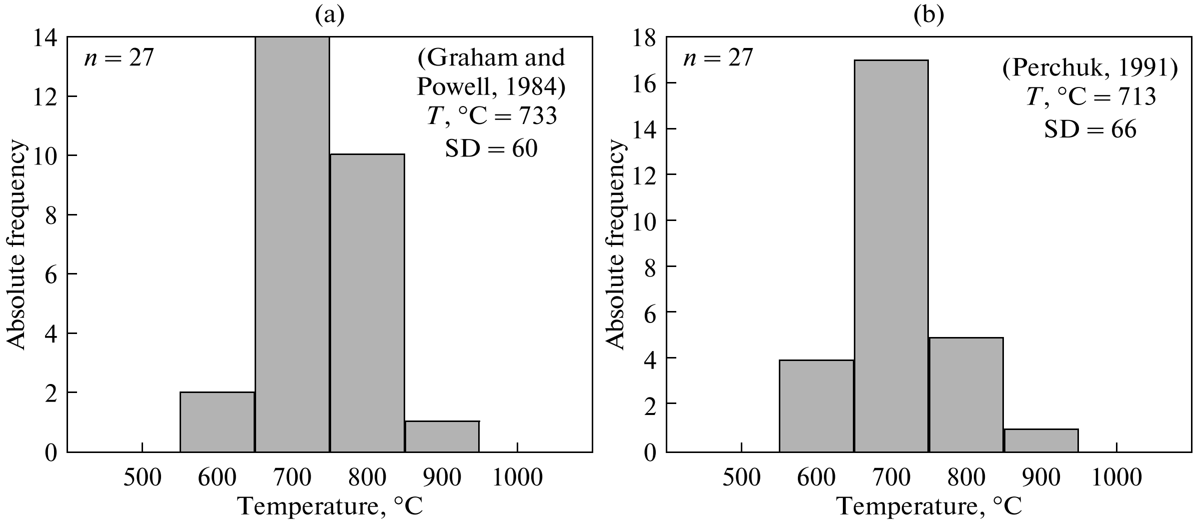

Fig. 7. Frequency histograms that summarize the results of the application of the garnet-hornblende thermometers of Graham and Powell (1984) and Perchuk (1991) to twenty seven (27) pairs.

Table 3. U-Th-Pb SHRIMP data for zircons from Thermes kyanite eclogite (sample RH506)

Spot	$^{206}Pb_c$, %	U, ppm	Th, ppm	$\frac{^{232}Th}{^{238}U}$	$^{206}Pb^*$, ppm	Age, Ma			±%	(1) $\frac{^{207}Pb^*}{^{206}Pb^*}$	±%	(1) $\frac{^{207}Pb^*}{^{235}U}$	±%	(1) $\frac{^{206}Pb^*}{^{238}U}$	±%	Rho
						(1) $\frac{^{206}Pb}{^{238}U}$		(1) $\frac{^{238}U}{^{206}Pb^*}$								
1	4.79	63	0.6	0.01	0.363	40.9	±1.7	157	4.1	0.047	56	0.041	56	0.00637	4.1	0.074
2	0.00	3	0.7	0.21	0.0304	67	±5.8	95.7	8.7	0.374	14	0.539	16	0.01045	8.7	0.532
3	0.00	9	0.5	0.05	0.0577	47.6	±4.9	135	10	0.177	14	0.181	17	0.00741	10	0.599
4	0.00	15	0.8	0.06	0.099	48.9	±2.3	131.2	4.7	0.11	12	0.115	13	0.00762	4.7	0.375
5	0.00	29	0.3	0.01	0.232	58.9	±2.1	108.9	3.6	0.051	12	0.0646	13	0.00918	3.6	0.277
6	0.00	56	1.8	0.03	0.41	55.1	±1.6	116.5	3	0.0497	9.1	0.0588	9.6	0.00858	3	0.310
7	0.00	40	0.3	0.01	0.224	41.7	±1.4	154.2	3.5	0.0473	11	0.0423	11	0.00649	3.5	0.306
8	0.00	41	1.8	0.04	0.233	42.2	±2.3	152.1	5.4	0.0459	11	0.0416	12	0.00657	5.4	0.430

Note: Errors are 1σ; Pb_c and Pb^* – indicate common and radiogenic portions, respectively. Error in standard calibration was 0.36% (not included in the above errors). Rho - error correlation (1) Common Pb-corrected using measured ^{204}Pb. The data were plotted on a Tera-Wasserburg diagram (Fig. 6b) because of the young ages obtained.

of domains with varying SiO_2 and Al_2O_3 chemical potentials. Formation of sapphirine, plagioclase, spinel and corundum symplectites during decomposition of kyanite crystals requires a mass-transfer process that would add MgO, FeO, CaO and Na_2O to kyanite. Kyanite is therefore chosen as the thermodynamic system of interest and the additional components are considered as independent unknowns. In other words, having kyanite as a starting point in the composition space and the symplectites of corundum, plagioclase, spinel and sapphirine as the final point, we can use compositional variables in a forward way to predict the conditions of formation of the observed mineral assemblage. The thermodynamic calculations were made using free-energy minimization (Connolly, 2005), the thermodynamic database of Holland and Powell (1998, revised 2002) and the mineral solution models summarized in Table 4. Water is excluded from the thermodynamic calculations since its presence would expand the stability field of hydrous phases and as a consequence would reduce the stability field of the phases constituting the pseudomorphs after kyanite. To illustrate the impact of the domain composition on the phases being formed after the decomposition of kyanite we will consider an example. In this example we assume that the composition of the system is allowed to vary linearly between pure kyanite and the composition of the corundum-plagioclase-spinel-sapphirine-bearing symplectites. The composition of the symplectites was calculated using the actual composition of these phases and their volume proportions (extrapolated from image analysis). Assuming initially that the breakdown of kyanite took place under isothermal conditions ($T = 750°C$) then, in order to form the symplectitic assemblage, kyanite would have to decompose below ~0.6 GPa otherwise garnet would have been formed in the pseudomorphs. The phase diagram (Fig. 9) predicts the formation of the symplectite paragenesis with the assumption that the composition of the kyanite domain varied continuously and linearly at constant temperature. This is a simplification that shows the development of corundum saturation by varying only MgO, FeO, CaO and Na_2O.

Modeling Strategy—the Full Picture

Systematic investigation of pressure, temperature and composition space (*P–T–X*) using forward modeling of equilibrium thermodynamics can yield the maximum range of *P-T* conditions within which the studied symplectites have been formed. In the model, equilibrium is assumed only between kyanite and adjacent phases. To illustrate the compositional phase relations relevant to the symplectitic paragenesis, we consider phase relations in isobaric-isothermal phase diagrams as a function of two compositional variables (i.e. *X–X* sections). In these diagrams, the origin represents an Al_2SiO_5 polymorph as a source of alumina and silica. Additive vectors represent the alkali addition (CaO + Na_2O—*y*-axis) and base metal oxide addition (FeO + MgO—*x*-axis) (Figs. 10a, 10b). The ratio of Al_2O_3/SiO_2 is treated as constant. Enrichment in Al_2O_3 would only change the amount of corundum predicted by calculated phase equilibria without changing the topology. On the other hand, enrichment in SiO_2 would suppress corundum

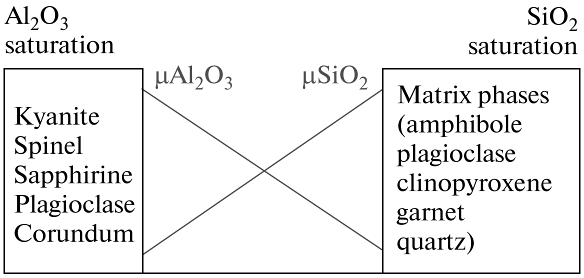

Fig. 8. Schematic diagram showing the domains of local chemical equilibrium. The symbol μ symbolizes the chemical potential.

Table 4. Solid-solution models used in thermodynamic calculations (for more details: http://www.perplex.ethz.ch/PerpleX_solution_model_glossary.html)

Mineral	Mineral Formula/Composition	Solution Model
Clinopyroxene	$Na_{y+w}[CaMg_xFe^{2+}_{(1-x)}]_{1-y-w}Al_y\,Fe^{3+}_w\,Si_2O_6$	Green et al., 2007
Orthopyroxene	$[Mg_xFe_{1-x}]_{2-y}Al_{2y}Si_{2-y}O_6$	Holland and Powell, 1996
Plagioclase	$Na_xCa_{1-x}Al_{2-x}Si_{2+x}O_8$	Newton et al., 1980
Garnet	$Fe_{3x}Ca_{3y}Mg_{3z}Mn_{3(1-x-y-z)}Al_2Si_3O_{12}$, $x + y + z \leq 1$	Holland and Powell, 1998
Spinel	$Mg_xFe_{1-x}Al_2O_3$	Holland and Powell, 1998
Sapphirine	$[Mg_xFe_{1-x}]_{4-y/2}Al_{9-y}Si_{2-y/2}O_{20}$	Holland and Powell, 1998
Cordierite	$Mg_{2x}Fe_{2y}Mn_{2(1-x-y)}Al_4Si_5O_{18} \cdot (H_2O)_z$, $x + y \leq 1$	Ideal

saturation and force quartz saturation. The latter can be rejected on the basis of textural evidence which demonstrates corundum saturation. The Na_2O/CaO and FeO/MgO ratios are constrained by mineral analyses. Since plagioclase and spinel are the only Na_2O–CaO and MgO–FeO bearing phases in the symplectitic domains respectively (sapphirine is not observed in all pseudomorphs and even when it is, its volume amount is minor), the variation of the aforementioned elements can be estimated by the composition and the amount of plagioclase and spinel in the pseudomorphs.

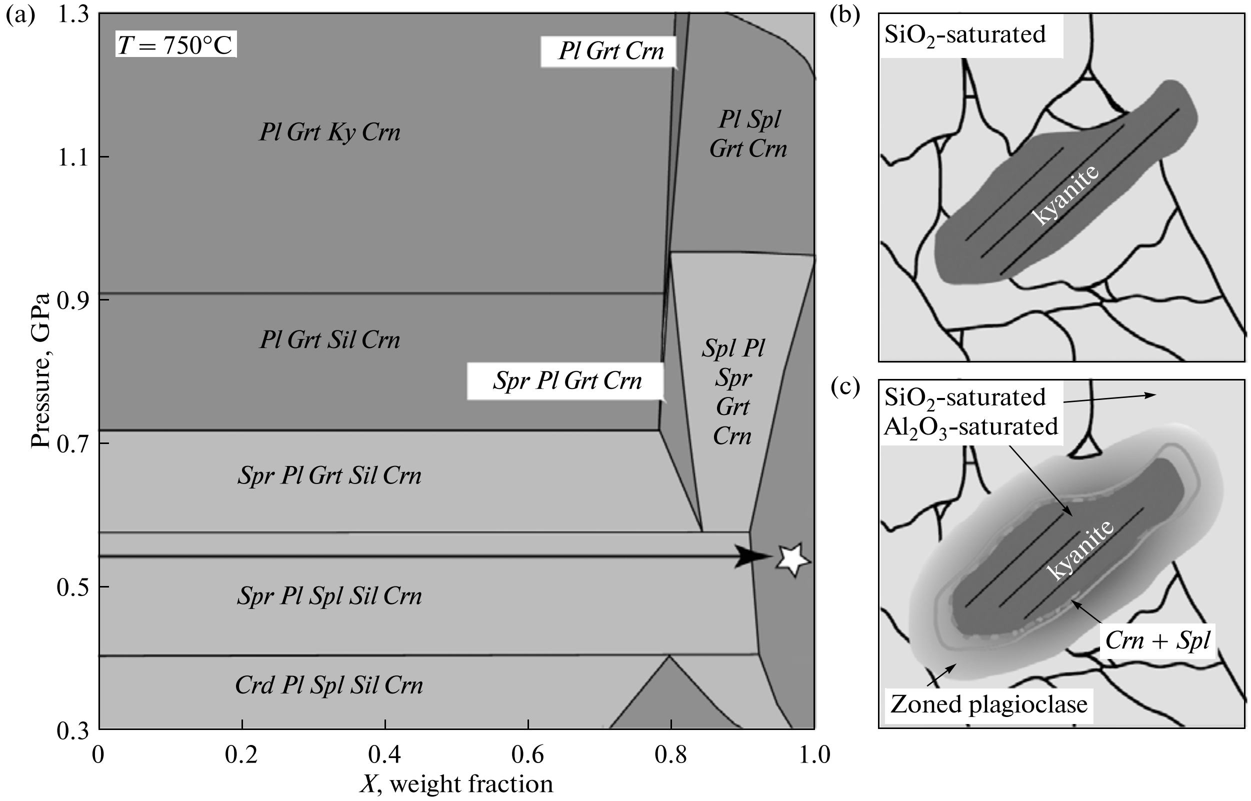

Fig. 9. (a) Pressure-composition (*P–X*) phase-diagram section showing the phase fields that have to be crossed during kyanite symplectitisation. The composition of the symplectite domain is in wt %: Na_2O: 4.540, CaO: 4.620, FeO: 6.230, MgO: 3.790, Al_2O_3: 44.525, SiO_2: 36.400 (at $X = 1$). The composition at $X = 0$ is the composition of pure kyanite and the composition at $X = 1$ is the composition calculated from its pseudomorph. Temperature was assumed to be 750°C, higher than the results from geothermometry (Fig. 7) in order to obtain a high-pressure limit during the symplectitisation process. Note that only at pressures below 0.6 GPa it is possible to form the symplectites with sapphirine, plagioclase corundum and spinel (indicated by a star) without forming garnet. (b) Schematic illustration showing the kyanite domain before and (c) after the beginning of symplectitisation. Note that kyanite is consumed to produce the sapphirine-corundum-spinel-plagioclase symplectites. The kyanite domain in (c) is saturated in corundum and is not in contact with the rest of the rock since a rim of zoned plagioclase has been formed. The dark colors of the rim illustrate relative anorthite abundance in the plagioclase. The thin lines mark the boundaries of the system.

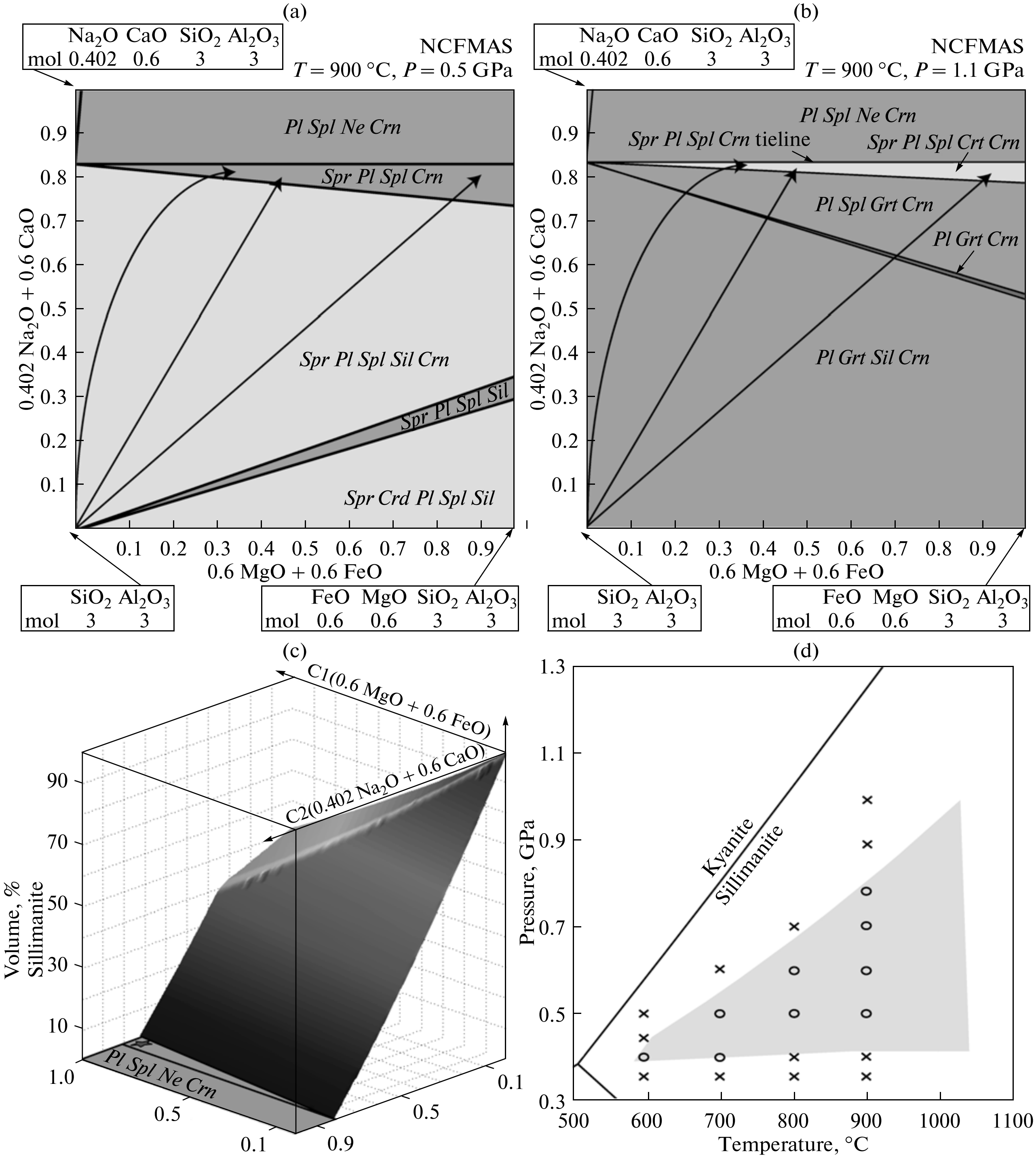

Fig. 10. *X–X* phase-diagram section calculated for the NCFMAS system and for fixed *P-T* conditions. Three arbitrarily chosen arrows show possible metasomatic paths from a pure aluminosilicate composition, that represents the initial composition of the kyanite domain (three moles of Al_2SiO_5), towards the plagioclase-sapphirine-spinel phase field for each diagram. No excess phases were assumed for these calculations. At low pressures ($P = 0.5$ GPa, $T = 900$°C) (a), adding MgO+FeO and Na_2O + CaO will consume the aluminosilicate phase resulting in the formation of sapphirine-corundum-plagioclase-spinel-bearing assemblages. (b) Same as in (a) but at higher pressures ($P = 1.1$ GPa, $T = 900$°C). Note that at higher pressures any continuous mass transfer would first form garnet until the aluminosilicate phase is consumed. (c) Calculated modal amount of the aluminosilicate phase (sillimanite in this case) from the diagram shown in (a). The mass-transfer path towards the observed symplectitic mineralogy (indicated here with a star) will consume the aluminosilicate phase. (d) A schematic *P-T* diagram showing the way the forward model has been set up. Composition-composition (*X–X*) phase-diagram sections (such as Figs. 10a, 10b) were calculated over a range of *P-T* conditions circles and crosses. The shaded field shown here represents the maximum *P-T* field for symplectite assemblage without garnet, orthopyroxene, and cordierite (runs with circles).

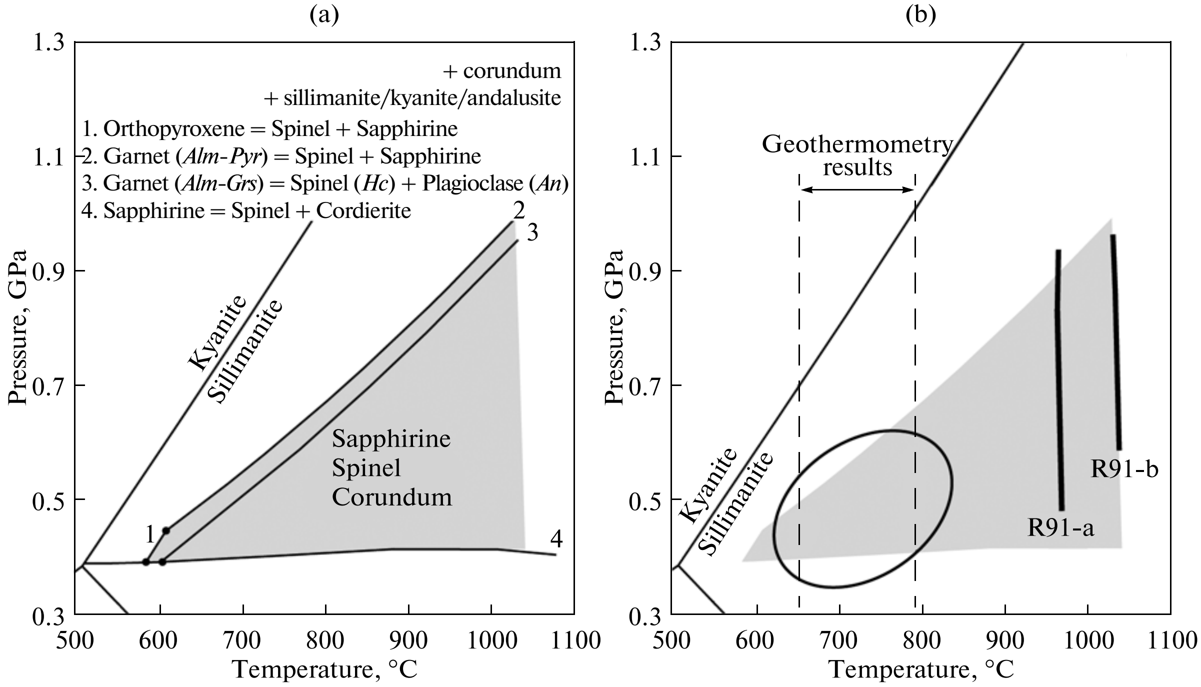

Fig. 11. (a) Calculated *P-T* projection after the analysis of the phase diagram section relations. Corundum and Al_2SiO_5 are assumed in excess as required from the *X–X* phase diagram sections. The univariant phase fields define limiting conditions for the symplectitisation of kyanite to produce sapphirine-spinel-corundum-plagioclase bearing assemblages. Note that the boundaries represent limiting conditions and have to be satisfied simultaneously. (b) Summarized results from thermometry (with uncertainty) and the thermodynamic modeling. The Lines R91-a and R91-b correspond to vapour absent solidus and the amphibole-out melting reaction of Rapp et al. (1991), respectively.

Corundum-spinel-sapphirine-plagioclase symplectites after kyanite can develop in any composition of the model system for which there is a continuous (not necessarily linear) path from the Al_2SiO_5 initial composition to the spinel-sapphirine-plagioclase-corundum field (see examples of possible paths in Figs. 10a, 10b). Along this path the Al_2SiO_5 phase is consumed, finally yielding a mineral assemblage consisting of spinel, plagioclase sapphirine and corundum (Fig. 10c). Although the mass-transfer path is unknown, it is constrained by the assumption that it did not cross phase fields where garnet or cordierite are produced since there is no textural evidence for their formation in the studied symplectitic domains. Several *X–X* phase diagram sections were therefore calculated for different *P*, *T*, Na_2O/CaO and MgO/FeO ratios to investigate the topology of the diagrams. Those which supported the petrographic observations were then used to infer the *P-T* conditions of formation of the symplectites (cf. Figs. 10a and 10b). The *P-T* conditions of formation of these symplectites were constrained by rejecting the conditions (i.e. diagrams like Fig. 10b) at which garnet, cordierite or pyroxene were produced during the breakdown of the Al_2SiO_5 phase (Fig. 10d).

Model Results

The phase relation analysis shows that, for bulk compositions consistent with the observed mineral assemblages, the *P-T* conditions at which the studied symplectites formed are bounded by the following univariant phase fields (Fig. 11a):

1) orthopyroxene = spinel + sapphirine,

2) garnet (*Alm-Prp*) = spinel + sapphirine,

3) garnet (*Alm-Grs*) = spinel (hercynite) + plagioclase (anorthite),

4) sapphirine = spinel + cordierite.

These four univariant fields (lines in the *P-T* space) in subsystems of the $Na_2O–CaO–FeO–MgO–Al_2O_3–SiO_2$ (NCFMAS) system are all saturated in corundum and an aluminosilicate (Al_2SiO_5) phase as predicted by the investigation of the *X–X* sections. Crossing any of these fields during metasomatism would produce minerals (orthopyroxene, garnet and cordierite) for which there is no textural or chemical evidence in the studied thin sections. For example, if the breakdown of the aluminosilicate phase (kyanite in this case) occurred above the limits imposed by reaction (2) garnet would have to be formed in order to produce sapphirine-spinel-plagioclase-corundum symplectites (Fig. 10b). The results of the modeling together with the thermometry results are illustrated in Fig. 11b. Within the uncertainty of the thermometry results, the upper pressure limit of the symplectite-forming process after kyanite is between 0.5 and 0.7 GPa. The *P-T* conditions predicted for the symplectite formation are within the stability field of sillimanite and not that of kyanite, which is observed in the rock. This is explained by the fact that kyanite is reacting non-isochemically to form the aforementioned symplectites (therefore it is not in its stability field) and phase equilibria using equilibrium thermodynamics do not account for the metastable preservation of mineral phases.

DISCUSSION

The studied symplectitic spinel, sapphirine, corundum and plagioclase were previously taken as evidence for high-pressure granulite-facies overprint (Liati and Seidel 1994; 1996). Our results show that these symplectites were formed at pressures much lower than 1.0 GPa, and temperatures <1050°C as required by the presence of stable amphibole in the rock. This is taken as a theoretical absolute upper-pressure limit. That the symplectites were formed under amphibolite-facies conditions (0.4 GPa $< P <$ 0.7 GPa, 580°C $< T <$ 800°C) is supported by the thermodynamic modeling which assumes local equilibrium (Fig. 11), the absence of granulite mineral assemblages, the geothermometry results (Fig. 7), and the metamorphic studies on country rocks (Krohe and Mposkos, 2002). The pressure difference of the estimated metamorphic pressures between Liati and Seidel (1996) and this work is at least 0.8 GPa.

The Eocene metamorphic age of 42 ± 2 Ma determined here by zircon geochronology for sample RH506 is equivalent to previous dating of similar kyanite eclogite lenses from the same Thermes area (Liati and Gebauer, 1999). However, our results are of consequence for deciding which metamorphic episode is responsible for the ages obtained. Liati and Gebauer (1999) suggested that their 42.2 ± 0.9 Ma zircon age dates eclogite formation at more than 60–70 km depth ($P >$ 1.9 GPa) in a subduction zone; the eclogites experienced granulite-facies thermal overprint (deduced by the presence of sapphirine) at 40.0 ± 1 Ma while the rocks were still at more than 1.5 GPa (> 50 km inferred depth), then were re-equilibrated at amphibolite-facies conditions (580–690°C/0.8–1.1 GPa; Liati and Seidel, 1996) before cooling down to 300°C at about 10 km depth at 36.1 ± 1.2 Ma (Liati and Gebauer, 1999). This age—metamorphic facies correlation implies extraordinary rates of exhumation and cooling, i.e. ~1.2 GPa and ~500°C within 4 Ma (from 40 to 36 Ma). In the light of our new P-T estimates, the formation of sapphirine symplectites after kyanite occurred at amphibolite-facies conditions and therefore large exhumation rates are not suggested. Additionally, high-pressure, Eocene eclogitic metamorphism occurs in the Cyclades, further south (Tomaschek et al., 2003; Lagos et al., 2007). Coeval eclogite-facies metamorphism in the Rhodope and in the Cyclades would require either north-dipping, double subduction during Eocene times (one in the south Aegean, one in the Rhodope Massif), or a single slab carrying the now ca. 400 km apart Rhodopean and Cycladic eclogites. Double subduction scenarios are difficult to reconcile with the single, continuous lithospheric slab imaged on seismic tomography of the Aegean region (Papazachos and Nolet, 1997; Bijwaard et al., 1998; Hafkenscheid et al., 2006). We note that the Eocene zircon ages are contemporaneous with intrusion of voluminous Tertiary granitoids throughout the Rhodope Massif (e.g. Soldatos et al., 2008) at the time of regional amphibolite-facies metamorphism (e.g. Liati, 1986). Therefore, our zircon metamorphic age most likely dates the closure of the U–Pb system by the end of the amphibolite-facies overprint (T ~ 720°C) that produced the sapphirine-bearing symplectites. Magmatism and metamorphism together indicate an important thermal flux in this region in the overriding plate above the Eocene Aegean slab. We conjecture that the 55–60 Ma concordant zircon ages obtained in our work refer to earlier cooling of the studied eclogite.

CONCLUSIONS

The geodynamic implications of the new P-T estimates show that during post-eclogite metamorphic overprint, the intermediate thrust units of the Rhodope Massif were at normal crustal depths. Kyanite eclogites from Thermes (Rhodope Massif) developed domains of quartz and corundum saturation which cannot be treated as a uniform system. The study of local equilibrium domains in metamorphic rocks involving composition and P-T as unknowns combined with geothermometry gives consistent results with previous regional studies for the overprint of the Thermes high-pressure rocks. This approach can be applied to different systems where mosaic equilibrium is observed and when the equilibration volume is not constrained due to mass transfer or metasomatism in general. We conclude that, when considering local thermodynamic equilibrium, the existing petrological data support that the Thermes kyanite-eclogite recorded a normal type of amphibolite-facies overprint during Eocene times.

ACKNOWLEDGMENTS

E.M. acknowledges Alexander S. Onassis Public Benefit Foundation for its financial support. D.K. was co-funded by the European Social Fund and National Resources—(EPEAEK TI PYTHAGORAS and the Kapodistrias Research Grant # 70/4/7622. The ETH-Zurich supports J-P.B. and J.C. Panagiotis Zachariadis is acknowledged for separating the zircons and preparing the zircon mount. Thomas Reischmann provided access to the EPMA facility at Mainz. We also thank Y. Podladchikov, M. Caddick, L. Tajčmanová and F. Schenker for comments and discussions that improved the manuscript. Leonid Aranovich is acknowledged for his constructive criticism and for editorial handling.

REFERENCES

Anderson, D.E. and Olimpio, J., Progressive homogenization of metamorphic garnets, south Morar, Scotland: evidence for volume diffusion, *Can. Mineral.*, 1977, vol. 15, pp. 205–216.

Aranovich, L.Ya. and Kozlovskii, V.M., The role of silica mobility in the formation of incipient eclogites, *Geochem. Int.*, 2009, vol. 47, no. 2, pp. 199–204.

Bijwaard, H., Spakman, W., and Engdahl, E.R., Closing the gap between regional and global travel time tomography, *J. Geophys. Res.*, 1998, vol. 103, no. B12, pp. 30055–30078.

Black, L.P., Kamo, S.L., Allen, C.M., Aleinikoff, J.N., Davis, D.W., Korsch, R.J., and Foudoulis, C., TEMORA 1: a new zircon standard for Phanerozoic U-Pb geochronology, *Chem. Geol.*, 2003, vol. 200, pp. 155–170.

Bonev, N., Burg, J.-P., and Ivanov, Z., Mesozoic–Tertiary structural evolution of an extensional gneiss dome-the Keshebir–Kardamos dome, eastern Rhodope (Bulgaria–Greece), *Int. J. Earth Sci. (Geol. Rundsch.)*, 2006, vol. 95, pp. 318–340.

Brun, J.-P. and Sokoutis, D., Kinematics of the Southern Rhodope Core Complex (North Greece), *Int. J. Earth Sci. (Geol. Rundsch.)*, 2007, vol. 96, pp. 1079–1099.

Burg, J.-P., Rhodope: From Mesozoic convergence to Cenozoic extension. Review of petro-structural data in the geochronological frame, *J. Virtual Explor.*, 2012, vol. 42, pp. 1–44.

Burg, J.-P., Ivanov, Z., Ricou, L.-E., Dimov, D., and Klein, L., Implications of shear-sense criteria for the tectonic evolution of the Central Rhodope massif, southern Bulgaria, *Geology*, 1990, vol. 18, pp. 451–454.

Burg, J.-P., Ricou, L.-E., Ivanov, Z., Godfriaux, I., Dimov, D., and Klein, L., Syn-metamorphic nappe complex in the Rhodope Massif. Structure and kinematics, *Terra Nova*, 1996, vol. 8, pp. 6–15.

Caddick, M.J., Konopásek, J., and Thompson, A.B., Preservation of garnet growth zoning and the duration of prograde metamorphism, *J. Petrol.*, 2010, vol. 51, 2327–2347.

Carswell, D.A., Eclogites and the eclogite facies: definitions and classification, in *Eclogite Facies Rocks*, Carswell, D.A., Ed., Glasgow: Blackie, 1990, pp. 1–13.

Connolly, J.A.D., Computation of phase equilibria by linear programming: a tool for geodynamic modeling and its application to subduction zone decarbonation, *Earth Planet. Sci. Lett.*, 2005, vol. 236, pp. 524–541.

Dale, J., Powell, R., White, R.W., Elmer, F.L., and Holland, T.J.B., A thermodynamic model for Ca–Na clinoamphiboles in Na_2O–CaO–FeO–MgO–Al_2O_3–SiO_2–H_2O–O for Petrological Systems, *J. Metamorph. Geol.,* 2005, vol. 23, pp. 771–791.

Dinter, D.A. and Royden, L., Late Cenozoic extension in northeastern Greece: Strymon Valley detachment system and Rhodope metamorphic core complex, *Geology*, 1993, vol. 21, pp. 45–48.

Ellis, D.J. and Green, D.H., An experimental study of the effect of Ca upon garnet–clinopyroxene Fe-Mg exchange equilibria, *Contrib. Mineral. Petrol.,* 1979, vol. 71, pp. 13–22.

Florence, F.P. and Spear, F.S., Effects of diffusional modification of garnet growth zoning on *P-T* path calculations, *Contrib. Mineral. Petrol.*, 1991, vol. 107, pp. 487–500.

Godard, G., Eclogites and their geodynamic interpretation: a history, *J. Geodynam.*, 2001, vol. 32, pp. 165–203.

Godard, G. and Mabit, J.-L., Peraluminus sapphirine formed during retrogression of a kyanite-bearing eclogite from Pays de Léon, Armorican Massif, France, *Lithos*, 1998, vol. 43, pp. 15–29.

Graham, C.M. and Powell, R., A garnet-hornblende geothermometer: calibration, testing, and application to Pelona Schist, Southern California, *J. Metamorph. Geol.*, 1984, vol. 2, pp. 13–31.

Green, E., Holland, T., and Powell, R., An order-disorder model for omphacitic pyroxenes in the system jadeite–diopside–hedenbergite–acmite, with applications to eclogitic rocks, *Am. Mineral.*, 2007, vol. 92, pp. 1181–1189.

Hafkenscheid, E., Wortel, M.J.R., and Spakman, W., Subduction history of the Tethyan region derived from seismic tomography and tectonic reconstructions, *J. Geophys. Res.*, 2006, vol. 111, p. B08401. Doi: 10.1029/2005JB003791.

Holdaway, M.J., Recalibration of the GASP geobarometer in light of recent garnet and plagioclase activity models and versions of the garnet–biotite geothermometer, *Am. Mineral.*, 2001, vol. 86, pp. 1117–1129.

Holland, T.J.B. and Powell, R., Thermodynamics of order–disorder in minerals: II. Symmetric formalism applied to solid solutions, *Am. Mineral.,* 1996, vol. 86, pp. 1425–1437.

Holland, T.J.B. and Powell, R., An internally consistent thermodynamic data set for phases of petrological interest, *J. Metamorph. Geol.*, 1998, vol. 16, pp. 309–343.

Jones, C.E., Tarney, J., Baker, J.H., and Gerouki, F., Tertiary granitoids of Rhodope, northern Greece: magmatism related to extensional collapse of the Hellenic Orogen?, *Tectonophysics*, 1992, vol. 210, pp. 295–314.

Kolocotroni, C. and Dixon, J.E., The origin and emplacement of the Vrondou granite, Serres, N.E. Greece, *Bull. Geol. Soc. Greece*, 1991, vol. 25, no. 1, pp. 469–483.

Korzhinskii, D.S., *Physico-Chemical Basis of the Analysis of the Paragenesis of Minerals*, New York: Consultants Bureau, 1959.

Koukouvelas, I. and Doutsos, T., Tectonic stages along a traverse cross cutting the Rhodopian zone (Greece), *Geol. Rundsch.*, 1990, vol. 79, no. 3, pp. 753–776.

Krohe, A. and Mposkos, E., Multiple generations of extensional detachments in the Rhodope mountains (northern Greece): evidence of episodic exhumation of high-pressure rocks, in *The Timing and Location of Major Ore Deposits in an Evolving Orogen*, Blundell, D.J., Neubauer, F., and Von Quadt, A., Eds., *Geol. Soc. London: Spec. Publ.*, 2002, vol. 204, pp. 151–178.

Lagos, M., Scherer, E.E., Tomaschek, F., Münker, C., Keiter, M., Berndt, J., and Ballhaus, C., High precision Lu-Hf geochronology of Eocene eclogite-facies rocks from Syros, Cyclades, Greece, *Chem. Geol.*, 2007, vol. 243, pp. 16–35.

Larionov, A.N., Andreichev, V.A., and Gee, D.G., The Vendian alkaline igneous suite of northern Timan: ion microprobe U-Pb zircon ages of gabbros and syenite, in *The Neoproterozoic Timanide Orogen of Eastern Baltica*, Gee, D.G. and Pease, V.L., Eds., *Geol. Soc. London Mem.*, 2004, vol. 30, pp. 69–74.

Liati, A., *Regional Metamorphism and Overprinting Contact Metamorphism of the Rhodope Zone, near Xanthi N. Greece: Petrology, Geochemistry, Geochronology*, Braunschweig, Tech. Univ., 1986.

Liati, A. and Gebauer, D., Constraining the prograde and retrograde *P-T-t* path of Eocene HP rocks by SHRIMP dating of different zircon domains: inferred rates of heating, burial, cooling, and exhumation for central Rhodope, Greece, *Contrib. Mineral. Petrol.*, 1999, vol. 135, pp. 340–354.

Liati, A. and Mposkos, E., Evolution of the eclogites in the Rhodope Zone of northern Greece, *Lithos*, 1990, vol. 25, pp. 89–99.

Liati, A. and Seidel, E., Sapphirine and högbomite in overprinted kyanite-eclogites of central Rhodope, N. Greece: first evidence of granulite-facies metamorphism, *Eur. J. Mineral.*, 1994, vol. 6, pp. 733–738.

Liati, A. and Seidel, E., Metamorphic evolution and geochemistry of kyanite eclogites in central Rhodope, northern Greece, *Contrib. Mineral. Petrol.*, 1996, vol. 123, pp. 293–307.

Lips, A.L.W., White, S.H., and Wijbrans, J.R., Middle–Late Alpine thermotectonic evolution of the southern Rhodope Massif, Greece, *Geodin. Acta*, 2000, vol. 13, pp. 281–292.

Ludwig, K.R., SQUID 1.12 A User's manual. A geochronological toolkit for Microsoft Excel, *Berkeley Geochronol. Cent. Spec. Publ.*, 2005(a), no. 2. www.bgc.org/klprogrammenu.html).

Ludwig, K.R., User's manual for ISOPLOT/Ex 3.22. A geochronological Toolkit for Microsoft Excel, *Berkeley Geochronol. Cent. Spec. Publ.*, 2005(b), pp. 1–71. www.bgc.org/klprogrammenu.html)

Mposkos, E.D. and Kostopoulos, D.K., Diamond, former coesite and supersilicic garnet in metasedimentary rocks from the Greek Rhodope: a new ultrahigh-pressure metamorphic province established, *Earth Planet. Sci. Lett.*, 2001, vol. 192, pp. 497–506.

Mposkos, E. and Liati, A., Metamorphic evolution of metapelites in the high-pressure terrane of the Rhodope zone, northern Greece, *Can. Mineral.*, 1993, vol. 31, pp. 401–424.

Nakamura, D. and Hirajima, T., Granulite-facies overprinting of ultrahigh-pressure metamorphic rocks, northeastern Su-Lu region, eastern China, *J. Petrol.*, 2000, vol. 41, pp. 563–582.

Newton, R.C., Charlu, T.V., and Kleppa, O.J., Thermochemistry of the high structural state plagioclases, *Geochim. Cosmochim. Acta,* 1980, vol. 44, pp. 933–941.

Papanikolaou, D. and Panagopoulos, A., On the structural style of Southern Rhodope, Greece, *Geol. Balc.*, 1981, vol. 11, no. 3, pp. 13–22.

Papazachos, C. and Nolet, G., P and S velocity structure of the Hellenic area obtained by robust nonlinear inversion of travel times, *J. Geophys. Res.*, 1997, vol. 102, no. B4, pp. 8349–8367.

Perchuk, L.L., Derivation of a thermodynamically consistent set of geothermometers and geobarometers for metamorphic and magmatic rocks, in *Progress in Metamorphic and Magmatic Petrology, a Memorial Volume in Honor of D.S. Korzhinskii*, Perchuk, L.L., Ed., Cambridge: University Press, 1991, pp. 93–111.

Powell, R. and Holland, T.J.B., On thermobarometry, *J. Metamorph. Geol.,* 2008, vol. 26, pp. 155–179.

Rapp, R.P., Watson, E.B., and Miller, C.F., Partial melting of amphibolite/eclogite and the origin of Archean trondhjemites and tonalities, *Precambrian Res.*, 1991, vol. 51, pp. 1–25.

Ricou, L.-E., Burg, J.-P., Godfriaux, I., and Ivanov, Z., Rhodope and Vardar: the metamorphic and the olistostromic paired belts related to the Cretaceous subduction under Europe, *Geodin. Acta*, 1998, vol. 11, no. 6, pp. 285–309.

Rushmer, T., Partial melting of two amphibolites: contrasting experimental results under fluid-absent conditions, *Contrib. Mineral. Petrol.*, 1991, vol. 107, pp. 41–59.

Siivola, J. and Schmid, R., *A Systematic Nomenclature for Metamorphic Rocks. 12. List of Mineral Abbreviations. Recommendations by the IUGS Subcommission on the Systematics of Metamorphic Rocks, 2007, Recommendations.* www.bgs.ac.uk/scmr/docs/papers/paper_12.pdf.

Sokoutis, D., Brun, J.-P., Van Den Driessche, J., and Pavlides, S., A major Oligo–Miocene detachment in southern Rhodope controlling north Aegean extension, *J. Geol. Soc. London*, 1993, vol. 150, pp. 243–246.

Soldatos, T., Koroneos, A., Kamenov, B., Peytcheva, I., von Quadt, A., Christofides, G., Zheng, X., and Sang, H., New U-Pb and Ar-Ar mineral ages for the Barutin–Buynovo–Elatia–Skaloti–Paranesti batholith (Bulgaria and Greece): refinement of its debatable age, *Geochem. Mineral. Petrol.-Sofia,* 2008, vol. 46, pp. 85–102.

Spear, F.S. and Florence, F.P., Thermobarometry in granulites: pitfalls and new approaches, *Precambrian Res.*, 1992, vol. 55, pp. 209–241.

Stacey, J.S. and Kramers, J.D., Approximation of terrestrial lead isotope evolution by a two-stage model, *Earth Planet. Sci. Lett.*, 1975, vol. 26, pp. 207–221.

Steiger, R.H. and Jäger, E., Subcommission on geochronology: convention on the use of decay constants in geo- and cosmochronology, *Earth Planet. Sci. Lett.*, 1977, vol. 36, pp. 359–362.

Tajčmanová, L., Konopásek, J., and Connolly, J.A.D., Diffussion-controlled development of silica-undersaturated domains in felsic granulites of the Bohemian Massif (Variscan belt of Central Europe), *Contrib. Mineral. Petrol.*, 2007, vol. 153, pp. 237–250.

Tajčmanová, L., Abart, R., Neusser, G., and Rhede, D., Growth of plagioclase rims around metastable kyanite during decompression of high-pressure felsic granulites (Bohemian Massif), *J. Metamorph. Geol.,* 2011, vol. 29, pp. 1003–1018.

Teipel, U., Eichhorn, R., Loth, G., Rohrmüller, J., Höll, R., and Kennedy, A., U-Pb SHRIMP and Nd isotopic data from the western Bohemian Massif (Bayerischer Wald, Germany): implications for Upper Vendian and Lower Ordovician magmatism, *Int. J. Earth Sci.(Geol. Rundsch.)*, 2004, vol. 93, pp. 782–801.

Tomaschek, F., Kennedy, A.K., Villa, I.M., Lagos, M., and Ballhaus, C., Zircons from Syros, Cyclades, Greece—recrystallization and mobilization of zircon during high-pressure metamorphism, *J. Petrol.*, 2003, vol. 44, pp. 1977–2002.

Wiedenbeck, M., Allé, P., Corfu, F., Griffin, W.L., Meier, M., Oberli, F., von Quadt, A., Roddick, J.C., and Spiegel, W., Three natural zircon standards for U-Th-Pb, Lu-Hf, trace element and REE analyses, *Geostand. Newslett.*, 1995, vol. 19, pp. 1–23.

Williams, I.S., U-Th-Pb Geochronology by ion microprobe, in *Applications in microanalytical techniques to understanding mineralizing processes*, *Rev. Econ. Geol.*, 1998, vol. 7, pp. 1–35.

Woodsworth, G.J., Homogenization of zoned garnets from pelitic schists, *Can. Mineral.*, 1977, vol. 15, pp. 230–242.

Wüthrich, E.D., *Low Temperature Thermochronology of the northern Aegean (Rhodope Massif)* Zürich: Swiss Federal Institute of Technology, 2009.